

pubs.acs.org/crystal Article

Traversing the Tightrope between Halogen and Chalcogen Bonds Using Structural Chemistry and Theory

Vinu V. Panikkattu, Anh Tran, Abhijeet S. Sinha, Eric W. Reinheimer, Emilie B. Guidez,* and Christer B. Aakeröy*



Cite This: *Cryst. Growth Des.* 2021, 21, 7168–7178



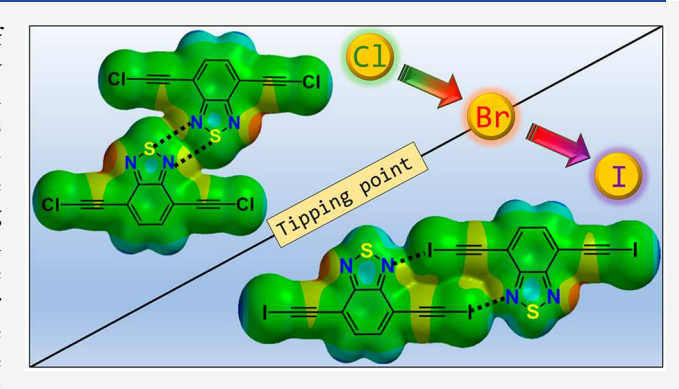
ACCESS

III Metrics & More

Article Recommendations

Supporting Information

ABSTRACT: Adjusting the physical and chemical properties of crystalline materials by controlling their structures is highly desirable in solid-state and materials chemistry. Such control can be achieved by carefully exploiting and fine-tuning the interactions between molecules. In this work, functionalized benzochalcogenadiazole molecules capable of forming two different σ -hole interactions (halogen and chalcogen bonds) are used as building blocks to assemble crystals with distinctly different structural features. *Ab initio* calculations are performed in order to rationalize the crystal structures obtained and to quantify the intermolecular interactions. It is found that the structural features and the balance between different interactions, as well as the relative strength of the σ -hole interactions, are highly sensitive to the identity of the



halogen and chalcogen atoms in the molecules. Both electrostatic/polarization and dispersion forces play an important role in defining the energetics of the chalcogen-bonded and halogen-bonded isomers, and by a control of the balance between these components, it is possible to precisely control the point at which one type of supramolecular architecture is favored over another.

■ INTRODUCTION

The a priori design of crystalline solids, with desirable structural features constructed by noncovalent interactions, represents a critical challenge in solid-state chemistry and materials science. 1-5 When these diverse interactions are forged into transferable protocols for programmable and hierarchical assembly, it may be possible to dial in structures and properties determined within the paradigm of "nanoarchitectonics". 7-9 Although hydrogen bonds have been the most widely utilized synthetic vectors for supramolecular synthesis, 10,11 halogen, 12,13 chalcogen, 14,15 and pnictogen bonds, $^{16-18}$ frequently referred to as " σ -hole" interactions, are gaining attention for more advanced and versatile synthetic methodologies. These bonds are all stabilized by a region of positive charge on the bridging atom that attracts a nucleophile. This electrostatic contribution can be complemented, to a greater or lesser extent, by charge transfer from the nucleophile into a σ^* antibonding orbital of the Lewis acid, as well as by polarization and dispersion. 19-21

The dramatic changes in length and energy scales that are inevitable in bottom-up approaches to materials synthesis can only be harnessed with the help of tools that operate in a synergistic manner with minimum mutual interference. ^{22–24} In order to identify synthetic protocols that simultaneously utilize halogen and chalcogen bonds for the assembly of molecular materials with specific structural features, we need to know

precisely how they may cooperate or compete in a system with multiple structural outcomes. ^{25,26} With that in mind, we have carried out a detailed experimental and theoretical study on a library of molecules that allows us to explore the delicate balance of strength and structural influence between halogen and chalcogen bonds.

In order to correlate small but controllable changes to the molecular structure, we opted for a core skeleton of a benzochalcogenadiazole. This fragment presents nitrogen atoms as potential acceptor sites for chalcogen-bond (ChB) donors (either sulfur or selenium). On the basis of existing structural data, the predominant interaction in the crystal structure of 2,1,3-benzothiadiazole is a chalcogen-bonded dimer.²⁷ However, upon the introduction of halogen atoms in the 4- and 7-positions, we set the stage for a competition that can lead to three postulated outcomes in the resulting crystal structure: a chalcogen-bonded dimer, a halogen-bonded (XB) dimer, or a hybrid of both (Scheme 1).

Received: September 4, 2021 Revised: October 20, 2021 Published: November 9, 2021





Scheme 1. Postulated Structural Outcomes Determined by the Balance between Chalcogen and Halogen Bonds

It is well-known that the increasing polarizability of heavier halogens/chalcogens enhances the magnitude of their σ -holes and consequently the strength of their respective intermolecular interactions. Furthermore, a halogen-bond donor can be activated through addition of an adjacent sphybridized carbon atom, and this gives us access to two families of compounds where we can independently and very precisely alter the strength of the competing interactions (Scheme 2).

Scheme 2. Library of Molecules Explored Computationally

"Green boxes indicate molecules that were also analyzed crystallographically. The crystal structures of S3, S4, and Te3 have been previously reported. 35-37 Se8 was successfully synthesized, but crystals suitable for single-crystal diffraction could not be obtained.

The results of this study may identify reliable supramolecular synthetic avenues for the assembly of crystalline molecular materials with predetermined metrics as well as for the generation of versatile protocols for translating intermolecular communication into blueprints for materials design.

■ EXPERIMENTAL SECTION

Procedures for the synthesis of S3, S4, S6–S8, Se3, Se4, and Se6–Se8 and their characterization (including ¹H, ¹³C, and ⁷⁷Se NMR and DSC) are described in Supporting Information. Solvents used to grow

the single crystals along with their crystallographic information are also described in the Supporting Information.

COMPUTATIONAL DETAILS

All calculations were performed with the GAMESS software package. $^{38-40}$ Geometry optimizations were performed at the RI-MP2 level of theory $^{41-43}$ in conjunction with a Def2-TZVP basis set. 44,45 An effective core potential was used for the tellurium and iodine atoms. 46 The monomers shown in Scheme 2 were optimized with $C_{2\nu}$ symmetry, whereas the halogen- and chalcogen-bonded dimers were optimized with C_{2h} symmetry. The energy decomposition analysis (EDA) scheme by Li et al. 47 was used to analyze dimer interaction energies at the MP2/Def2-TZVP level of theory. The Boys and Bernardi counterpoise (CP) correction was applied to correct the basis set superposition error. 48 It is noted that the RI-MP2/Def2-TZVP methods have been commonly used in modeling σ -hole interactions $^{49-51}$ and proved to yield energies comparable to those of CCSD(T). 52

RESULTS

Nonactivated Sulfur Compounds S1-S4. Fluorine-substituted S1 and chlorine-substituted S2 were only explored computationally.

The crystal structure of \$3³⁶ shows the presence of a ChB dimer (Figure 1a) with an S---N distance of 3.226(4) Å and a

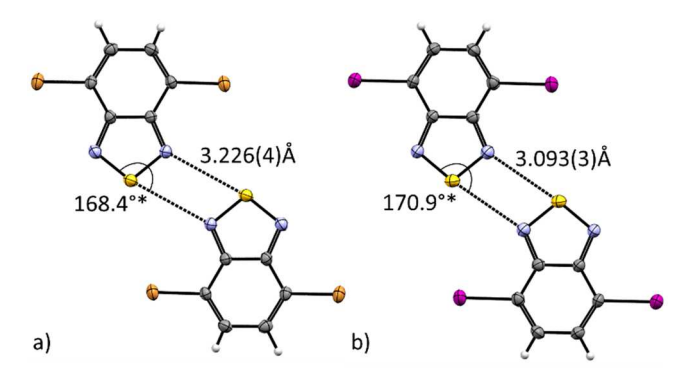


Figure 1. Primary intermolecular interactions in each crystal structure showing a ChB dimer in (a) S3 and (b) S4. The asterisks indicate that the esds are unavailable.

4% reduction in combined van der Waals (vdW) radii,⁵³ along with a separate ChB zigzag vertical chain (Figure 2) having a distance of 3.238(4) Å and a 3% reduction in combined vdW radii. It also contains two type II Br---Br short contacts,⁵⁴ 3.542(1) and 3.662(1) Å, with 4% and 1% reductions in their combined vdW radii, respectively.

The crystal structure of \$4³⁵ contains a similar ChB dimer (Figure 1b) but with a shorter S---N distance of 3.093(3) Å and an increased reduction, 8%, in combined vdW radii, along with a type II I---I short contact at 3.789(1) Å with a 4% reduction in vdW radii.

Quantum chemical calculations on the ChB dimers S1-S4 show that the interaction energies increase by ~ 1.4 kcal/mol from F to I (Table 1), whereas the intermolecular S---N distances remain nearly constant. Computed intermolecular distances are underestimated in comparison to those in experiments, possibly because the computations are done in the vacuum phase and do not account for the solid-state environment. The stronger chalcogen bond with increasing halogen atom size is driven by an increase in dispersion energy

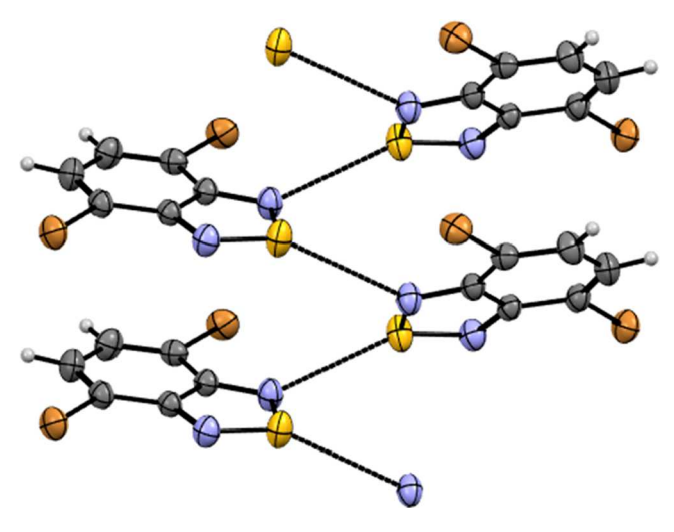


Figure 2. Chalcogen-bonded zigzag chain in S3.

Table 1. CP-Corrected MP2/Def2-TZVP Interaction Energies ΔE (in kcal/mol), RI-MP2/Def2-TZVP Intermolecular Distances R (in Å), and Angles θ (in deg) of Nonactivated Chalcogen-Bonded (ChB) and Halogen-Bonded (XB) Dimers S1–S4

		ChB dime	r		XB dime	r
Target	ΔE	R^a	θ^{b}	ΔE	R [€]	$ heta^d$
S1	-5.58	3.01	173.91	N/A	N/A	N/A
S2	-6.39	2.99	173.51	-2.61	3.26	164.37
S3	-6.76	2.99	173.79	-3.30	3.33	160.72
S4	-6.95	2.99	174.98	-3.54	3.49	156.00
^a SN di	stance. ^b N	IS–N a	ngle. ^c X]	N distance	e. dC-X-	N angle.

(about 3 kcal/mol), which may be due to a larger polarizability of the halogen atom (Figure 3 and Table S1).

The corresponding XB dimer interaction energies are roughly half in value, increasing by ~0.9 kcal/mol from Cl

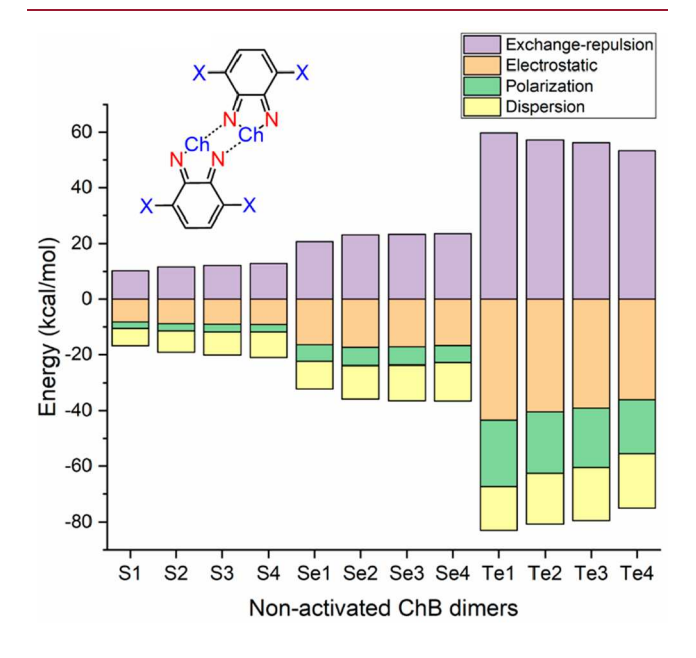


Figure 3. Energy decomposition of nonactivated ChB dimers (MP2/Def2-TZVP).

to I (Table 1). We note that, since fluorine does not have a positive σ -hole potential (Table S11),³⁰ a halogen-bonded dimer could not be optimized. Electrostatic/polarization and dispersion forces increase by 3.0 and 2.1 kcal/mol, respectively (Figure 4 and Table S1). The former results from the

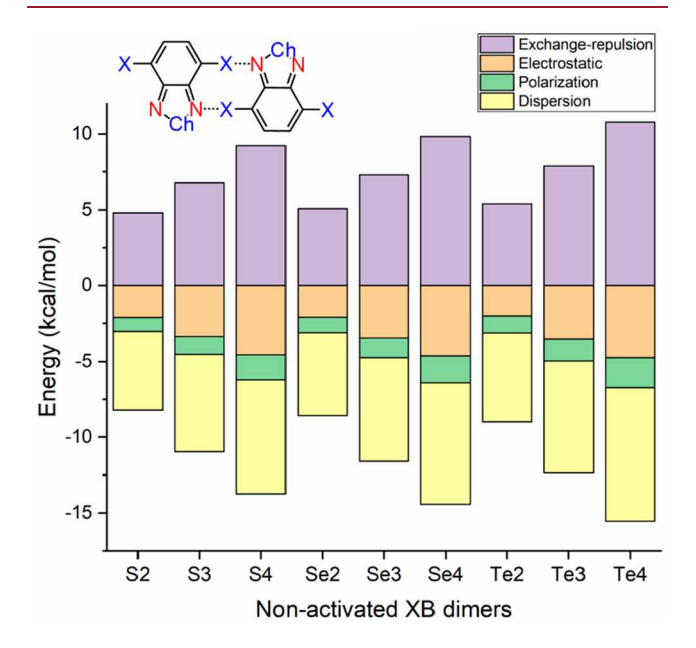


Figure 4. Energy decomposition of nonactivated XB dimers (MP2/Def2-TZVP). Due to the absence of a positive σ -hole potential, halogen-bonded structures could not be optimized for fluorine-substituted targets.

increasingly large electrostatic potential at the σ -hole³⁰ (cf. the Supporting Information), whereas the latter is due to the larger polarizability of the halogen atom. The C–X---N angle becomes less linear as the halogen atom becomes larger (Table 1). We hypothesize that, since the σ -hole becomes larger with increasing halogen atom size, such a misalignment has a small effect on the strength of the electrostatic σ -hole interaction. However, it can reduce the X–X repulsion between halogen atoms on neighboring molecules involved in forming the XB dimer. This hypothesis is consistent with the large increase in the exchange-repulsion energy (4.2 kcal/mol) observed upon moving from Cl to I (Figure 4 and Table S1).

Nonactivated Selenium Compounds Se1-Se4. Fluorine-substituted Se1 and chlorine-substituted Se2 were only explored computationally.

The crystal structure of Se3 (where X = Br) displays the same ChB dimer as was found in the nonactivated sulfur series, with a Se---N bond distance of 2.942(1) Å and a 15% reduction in the combined vdW radii (Figure 5a), along with a quasi type I Br---Br short contact with a distance of 3.525(1) Å and a 5% reduction in combined vdW radii.

The Se---N bond distance in **Se4** is 2.911(2) Å with a 16% reduction in combined vdW radii (Figure 5b). Also present is a type II I---I short contact measuring 3.796(2) Å with a 4% reduction in combined vdW radii.

Quantum chemical calculations for the ChB selenium targets Se1-Se4 show that the interaction energies increase by ~ 1.3 kcal/mol on going from F to I (Table 2), whereas the intermolecular distances do not vary significantly. Similar to the sulfur compounds, dispersion forces are mostly responsible for this overall increase (Figure 3 and Table S2). We note that,

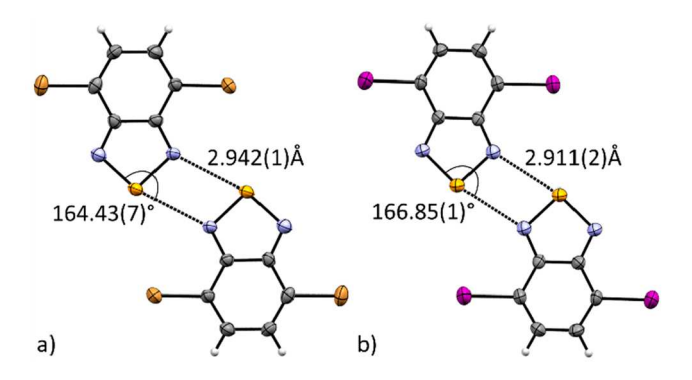


Figure 5. Primary interactions in each crystal structure showing a ChB dimer in (a) Se3 and (b) Se4.

Table 2. CP-Corrected MP2/Def2-TZVP Interaction Energies ΔE (in kcal/mol), RI-MP2/Def2-TZVP Intermolecular Distances R (in Å), and Angles θ (in deg) of Nonactivated Chalcogen-Bonded (ChB) and Halogen-Bonded (XB) Dimers Se1–Se4

	(ChB dime	•		XB dime	r
Target	ΔE	R^a	θ^{b}	ΔE	R^c	$ heta^d$
Se1	-9.93	2.87	166.36	N/A	N/A	N/A
Se2	-11.02	2.86	166.75	-2.63	3.24	164.86
Se3	-11.37	2.87	167.50	-3.40	3.31	161.19
Se4	-11.25	2.89	169.09	-3.58	3.47	156.46
^a SeN c	listance. ^b N	Se-N	angle. cX	-N distanc	e. ^d C–X-	N angle.

unlike the sulfur systems, the total interaction energy slightly decreases on switching from X = Br to X = I. This is likely due to the large steric repulsion between the neighboring selenium and iodine atoms (cf. the Discussion).

The Se---N interactions in the ChB dimers are about 4 kcal/mol stronger than the corresponding S---N interactions (Tables 1 and 2). In agreement with this observation, the Se---N bond is shorter than the S---N bond. This behavior is consistent with the stronger σ -hole interaction for larger chalcogen atoms (cf. the Supporting Information). In fact, the electrostatic/polarization interaction is about 12 kcal/mol larger for Ch = Se than for Ch = S, consistent with the larger Mulliken charges on the chalcogen and nitrogen atoms (Figure 3 and Tables S2 and S11). The larger Se atom is also more polarizable than the sulfur atom, therefore yielding higher dispersion energies.

The corresponding halogen-bonded dimer interaction energies are roughly a third in value, increasing by ~ 1.1 kcal/mol on going from Cl to I (Table 2). Unsurprisingly, the strengths of the intermolecular forces are similar to those computed for the sulfur compounds S1–S4 (Figure 4 and Table S2).

Nonactivated Tellurium Compounds Te1–Te4. The tellurium compounds are synthetically challenging, and similar tellurium heterocycles are known to be highly unstable⁵⁷ with poor solubilities, limiting their solution- and solid-state characterization.³⁷ Therefore, the experimental study of this series is limited to the previously reported Te3³⁷ crystal structure coupled with a detailed computational analysis.

The crystal structure of Te3 displays the previously seen Ch-N dimer interaction with a Te---N chalcogen bond distance of 2.697(8) Å and a 25.3% reduction in its combined vdW radii, which is the highest for a chalcogen bond for any

target explored in this study (Figure 6). A new feature of this tellurium series is that the second σ -hole of the same Te atom,

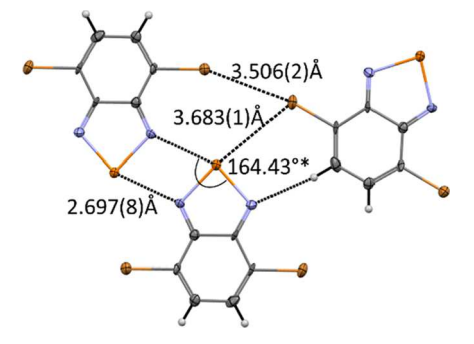


Figure 6. Primary intermolecular interactions in the crystal structure of **Te3** showing a ChB dimer. The asterisk indicates that the esd is unavailable.

which is much larger than the corresponding sulfur or selenium σ -hole (Figure S1), also forms a chalcogen bond with the electron-rich equator of the bromine atom, with a bond distance of 3.683(1) Å and a 5.8% reduction in its combined vdW radii. That same bromine atom in turn also forms a type I Br–Br halogen short contact with a distance of 3.506(2) Å and a 5.2% reduction in its combined vdW radii.

Interaction energies and structural data of ChB and XB dimers are shown in Table 3. The EDA is shown in Table S3.

Table 3. CP-Corrected MP2/Def2-TZVP Interaction Energies ΔE (in kcal/mol), RI-MP2/Def2-TZVP Intermolecular Distances R (in Å), and Angles θ (in deg) of Nonactivated Chalcogen-Bonded (ChB) and Halogen-Bonded (XB) Dimers Te1–Te4

		ChB dimer			XB dimer				
Target	ΔE	R^a	θ^b	ΔE	R^c	θ^d			
Te1	-20.74	2.67	156.37	N/A	N/A	N/A			
Te2	-20.88	2.71	158.41	-2.67	3.23	165.39			
Te3	-20.70	2.73	159.58	-3.51	3.29	161.74			
Te4	-19.46	2.77	161.59	-3.66	3.45	157.11			
^a TeN angle.	distance.	^b NTe-N	angle.	^c XN	distance.	^d C-XN			

Unlike Ch = S & Se, the interaction energy of the chalcogen-bonded dimer decreases with increasing halogen size, consistent with an increasingly large Te---N bond distance. Similar to Ch = S & Se, the dispersion energy increases by 4 kcal/mol as we go from X = F to X = I (Table S3). However, in contrast to the smaller chalcogen atoms, the electrostatic/polarization energy *decreases* by 12 kcal/mol in that order. This trend can be readily explained by the structural rearrangement of the monomers that is necessary to reduce the large steric repulsion between the adjacent Te---X atom and Te---Te atom pairs, as seen from its increasing percent overlap in their vdW radii (Table S13; cf. the Discussion).

The interaction energies of the chalcogen-bonded dimers are nearly twice as large for Ch = Te than for Ch = Se, which is also reflected in the shorter Te---N distances in comparison to the Se-N distances (Tables 2, 3, and S13). This stronger interaction can be explained by the higher positive charge on tellurium, giving a much larger electrostatic/polarization energy (Figure 3 and Tables S3 and S11). In addition, the

larger tellurium atom is also more polarizable, yielding higher dispersion energies. Finally, it is observed that the NCh–N angle decreases in the order S > Se > Te, which can be explained by the larger area of the σ -hole in that order allowing for increased rearrangement to reduce steric repulsion (Figure S1 and S4, Table S13).

The corresponding XB dimer interaction energies are approximately a fifth in value and similar to those obtained for Ch = S & Se. Geometries for these systems are also similar to those observed for Ch= S & Se (Figure 4, Table S3).

Activated Sulfur Compounds S5-S8. Fluorine-substituted S5 was only explored computationally. The chlorinesubstituted activated S6 produced two different polymorphs. Form 1 (S6I, Figure 7a) contains a ChB dimer with a S---N distance of 3.062(2) Å and a considerable 9% reduction in combined vdW radii, which represents the shortest ChB in the sulfur series. Interestingly, the second nitrogen atom of the same thiadiazole moiety forms part of a previously unseen Cl---N halogen bond measuring 3.160(2) Å with a 4% reduction in its combined vdW radii. Form 2 (S6II, Figure 7b) contains a ChB dimer with a longer S---N distance measuring 3.308(3) Å with a 1% reduction in combined vdW radii, which is the longest ChB in the sulfur series. The second nitrogen atom of the same thiadiazole moiety takes part in a Cl---N halogen bond, 3.143(3) Å, with a 5% reduction in combined vdW radii. That same chlorine atom also forms a Cl---C≡C halogen bond measuring 3.434(4) Å with a 0.6% reduction in combined vdW radii.

The crystal structure of \$7 was particularly challenging. Qualitative analyses of each atom's temperature factors suggested that all three molecules in the asymmetric unit were disordered. Splitting of the individual atoms or the reorientation of each molecule in Olex2 to wholly assign the disordered components coupled with bond distance restraints did not yield successful refinement results. The secondary (or in some cases tertiary) positions of the atoms from the three disordered molecules in the asymmetric unit were found in the difference map. After they were renamed, the atoms at each site were assigned to parts and reasonable occupancy ratios assigned to resolve as much residual electron density as possible. Suitable bond distances, thermal parameters, and molecular orientations were achieved via the application of the RIGU, SADI, and EADP constraints and restraints.

Changing the halogen atom from Cl to Br in \$7 disrupts the previously dominant ChB dimer (Figure 7c). While the relative orientation of molecules in \$7 is similar to that in \$6, which forms a ChB dimer, only one S---N pair forms a chalcogen bond with a representative distance of 3.295(6) Å and a 2% reduction in its combined vdW radii, along with a S---C=C short contact from the same S atom measuring 3.320(6) Å with a \$5.1% reduction in combined vdW radii. The other S---N pair is separated farther than their combined vdW radii and thus is not interacting. The second nitrogen atom of the thiadiazole moiety forms the previously seen X---N halogen bond with a representative Br---N bond length of 3.266(6) Å and a 4% reduction in its combined vdW radii. There also exists a Br---C=C halogen bond measuring 3.259(5) Å with an 8% combined reduction in its combined vdW radii.

In the structure of the iodo-substituted S8 (Figure 7d), however, a considerable structural change has taken place, in the form of the postulated XB dimer (Scheme 1) with a I---N halogen bond measuring 3.086(3) Å with a 12.6% reduction in its combined vdW radii. The second nitrogen atom forms a S---

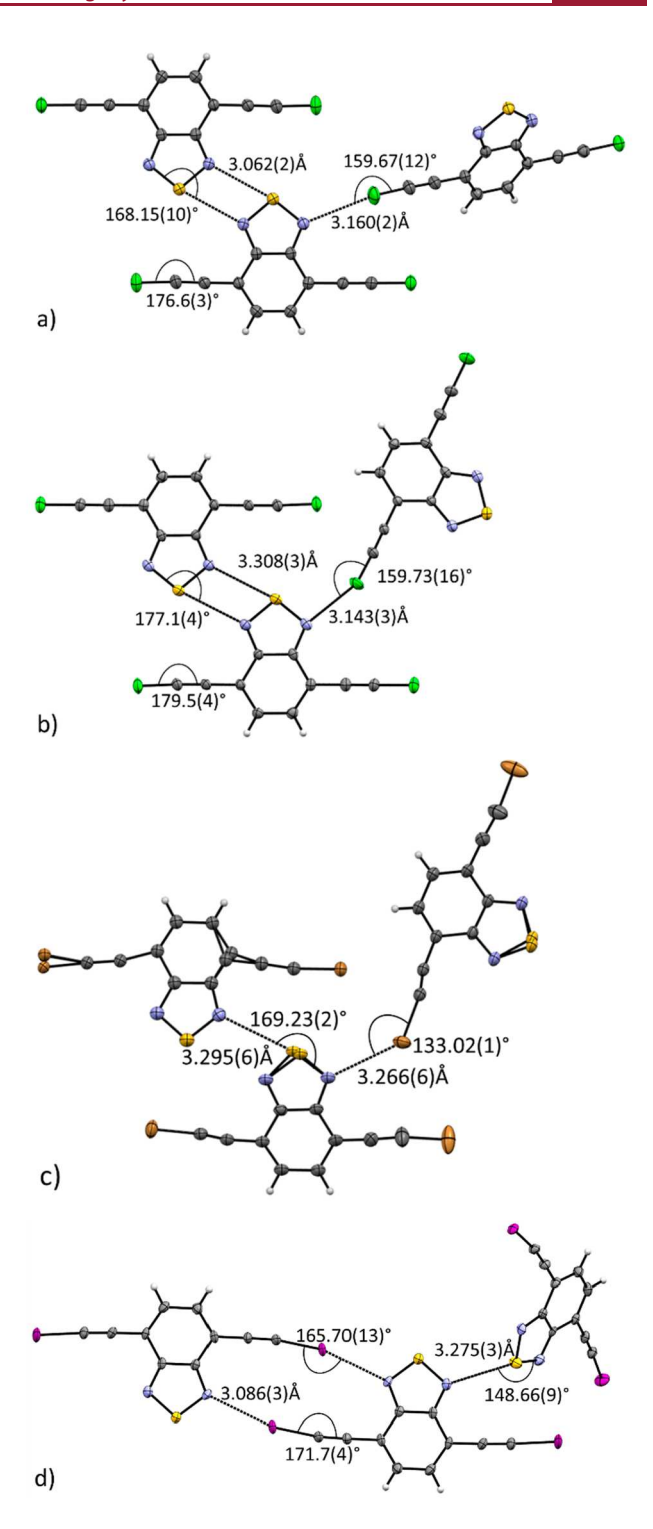


Figure 7. Primary interactions in each crystal structure showing a ChB dimer in polymorphs (a) S6I and (b) S6II, breaking of the ChB dimer in (c) S7, and the formation of a XB dimer in (d) S8.

N chalcogen bond measuring 3.275(3) Å with a 2.2% reduction in its combined vdW radii. At the same time, the second iodine atom forms a I---C≡C halogen bond, 3.440(4) Å, with a 7% reduction in combined vdW radii.

Quantum chemical calculations for the chalcogen-bonded dimers show that the interaction energies increase by \sim 2.3 kcal/mol on going from F to I (Table 4), whereas the intermolecular distances remain constant. These trends are

Table 4. CP-Corrected MP2/Def2-TZVP Interaction Energies ΔE (in kcal/mol), RI-MP2/Def2-TZVP Intermolecular Distances R (in Å) and Angles θ (in deg) of Activated Chalcogen-Bonded (ChB) and Halogen-Bonded (XB) Dimers S5–S8^a

	ChB dimer			XB dimer			
Target	ΔE	R^{b}	θ^c	ΔE	R^d	θ^e	θ^{f}
S 5	-6.30	2.99	173.20	-1.37	3.17	164.30	179.89
S6	-7.57	2.99	171.63	-5.45	3.11	166.04	177.48
S 7	-8.11	2.99	171.39	-7.17	3.10	165.87	175.29
S8	-8.63	2.99	171.36	-9.37	3.09	165.77	171.67

"Interaction energies highlighted in boldface point to the switch in the most stable dimer from the ChB dimer to the XB dimer in S8. b S---N distance. "N---S-N angle. "X---N distance." XB angle. f C \equiv C-X bend angle.

similar to what was observed for the nonactivated systems. This increase in energy is mostly due to dispersion forces, which become stronger as the halogen atoms become larger (Figure 8 and Table S4). We note that, unlike the nonactivated

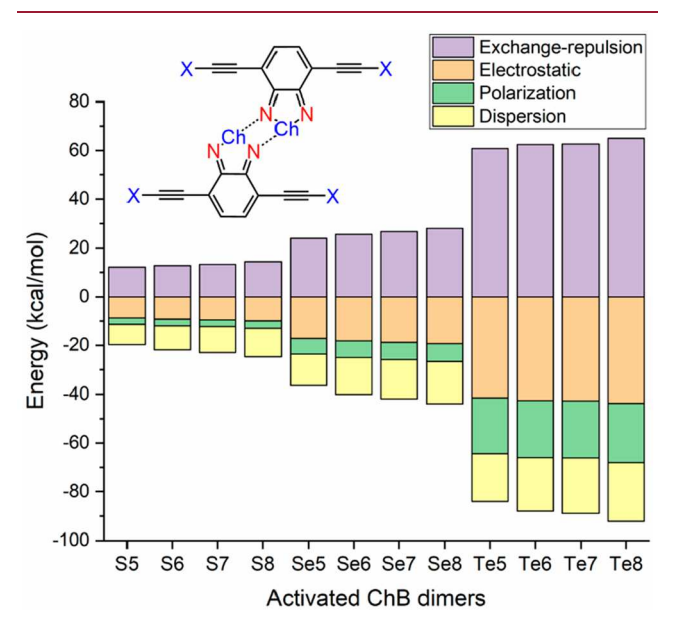


Figure 8. Energy decomposition of activated ChB dimers (MP2/Def2-TZVP).

systems, a reduction in the N---Ch—N angle is observed with increasing halogen size (Tables 1 and 4). In addition, this angle is up to about 3.5° smaller for these activated dimers than for the nonactivated dimers. We propose that this is due to the lack of repulsion between the adjacent S---X atom pairs (Figure S4).

An interesting feature in the activated series is the optimization of a halogen-bonded dimer with X = F, such as in S5 (Figure S3), despite the absence of any significant σ -hole on the fluorine atom (Figure S2, Table S11). An energy decomposition analysis for the activated sulfur XB dimers (Figure 9 and Table S4) shows that the formation of the halogen-bonded dimer for X = F is driven by dispersion forces (-3.03 kcal/mol), whereas electrostatic forces are negligible (-0.21 kcal/mol). Therefore, this F---N "bond" is not a conventional halogen bond driven by a σ -hole interaction.

The halogen-bonded dimer interaction energy steadily increases by about 4 kcal/mol upon moving from Cl to I (Table 4). This energy increase is much larger than that found for the nonactivated systems (Table 1). In addition, the energy decomposition analysis shows that the electrostatic/polarization components of the interaction energy for X = Cl, Br, I

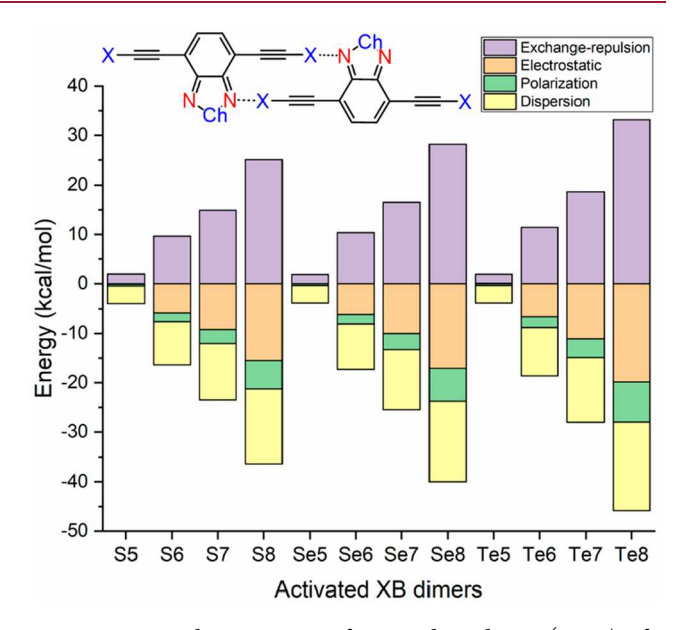


Figure 9. Energy decomposition of activated XB dimers (MP2/Def2-TZVP).

are about 3–4 times larger than for the nonactivated systems (Tables S1 and S4 and Figures 4 and 9). These data are consistent with the more positive Mulliken charges on the halogen atoms and the larger electrostatic potentials of the σ -hole in comparison to those in the nonactivated systems (Table S11; cf. the Supporting Information).

Unlike the case in in the nonactivated systems, the XB dimer is energetically comparable to the ChB dimer. As shown in Table 4, the C-X---N halogen bond angle increases from 164.3° for F in S5 to 165.8° for I in S8. This is possible because the attached intramolecular C≡C-X triple bond angle bend increases considerably from the original relatively linear 179.9° in S5 to 171.7° in S8 as we go from F to I. For S8 with Ch = S and X = I, the halogen-bonded dimer interaction energy in fact becomes slightly larger than that of the chalcogen-bonded dimer (Table 4), which is consistent with the XB dimer observed in the crystal structure of S8 (Figure 7d). We also note that the computed intramolecular $C \equiv C - I$ bend angle in S8 at 171.7° (Table S14) is extremely close to that observed experimentally at 171.7(4)° (Figure 7d). The purpose of the bending is to maximize the highly directional σ hole interaction while minimizing repulsion between the alkyl chains. It is worth pointing out that, without this C≡C-I bending, the halogen-bonded dimer would, in fact, have a lower interaction energy than the corresponding chalcogenbonded dimer (Table S14; cf. the Supporting Information).

Activated Selenium Compounds Se5—Se8. The fluorine-substituted compound Se5 was only explored computationally.

The crystal structure of the chlorine-substituted **Se6** (Figure 10a) presents a Se---N ChB dimer with a distance of 2.966(3)

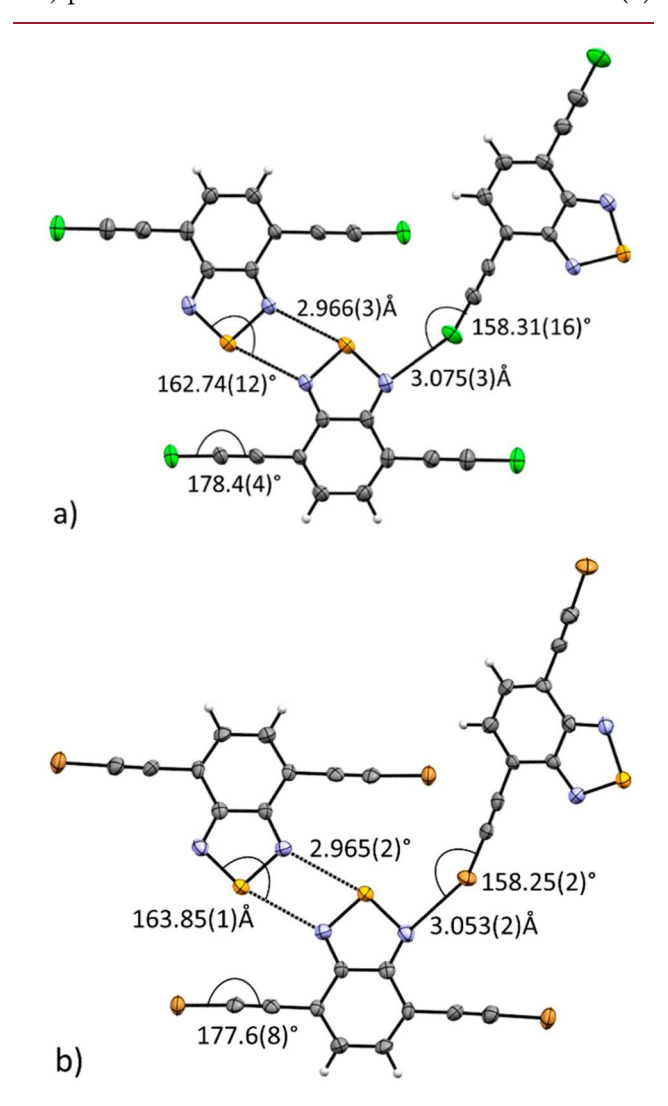


Figure 10. Primary interactions in each crystal structure showing a ChB dimer in (a) Se6 and (b) Se7.

Å and a 14.0% reduction in combined vdW radii, while the other nitrogen atom of the selenadiazole moiety forms a Cl---N halogen bond, 3.075(3) Å, with a 6.8% reduction in combined vdW radii. A second chlorine atom also forms a Cl---C≡C

halogen bond measuring 3.417(4) Å with a 1% reduction in combined vdW radii.

The bromo-substituted Se7 is isostructural with Se6 (Figure 10b). The ChB dimer has a Se---N distance of 2.965(2) Å with a 14.1% reduction in combined vdW radii, while the second nitrogen atom of the thiadiazole moiety takes part in a Br---N halogen bond, 3.053(2) Å, with a 10.2% reduction in combined vdW radii. A second bromine atom also participates in a Br---C≡C halogen bond measuring 3.398(2) Å with a 4% reduction in combined vdW radii.

Although we successfully synthesized **Se8**, we were unable to grow single crystals suitable for single-crystal diffraction despite considerable efforts.

Quantum chemical calculations for the chalcogen-bonded systems show that the interaction energies increase by \sim 3 kcal/mol on going from F to I (Table 5), whereas the intermolecular distances do not vary significantly. Similar to the nonactivated systems, the interaction energy of the ChB dimers is larger for Ch = Se than for Ch = S (Tables 4 and 5). We note that, unlike the nonactivated systems, the interaction energy continuously increases with halogen size (Tables 2 and 5). In addition, the N---SeN angle does not increase as the halogen size becomes larger. We propose that these trends are due to the absence of steric repulsion between the neighboring chalcogen and the halogen atom that occur in the nonactivated dimers (cf. the Discussion).

The corresponding halogen-bonded dimer interaction energies increase by \sim 4.0 kcal/mol on going from Cl to I, consistent with a decreasing intermolecular distance (Table 5). The directional σ -hole interaction is enhanced in these activated systems compared to that in the nonactivated systems. As before, the optimized halogen-bonded dimer for X = F is due to dispersion forces, not electrostatic interactions (Figure 8 and Table S5).

Activated Tellurium Compounds Te5–Te8. The general chemical instability of the tellurium compounds meant that they were only examined using a detailed computational analysis. As observed for Ch = S & Se, the ChB dimer interaction energy increases in the order F < Cl < Br < I, mostly due to gradually increasing dispersion energies (Figure 8 and Table S6). In addition, the interaction energy for the ChB dimer increases in the order S < Se < Te, mostly due to more prominent electrostatic σ -hole interactions (Table 6).

The XB dimers behave similarly to those in the Ch = S, Se series, showing that the nature of the chalcogen atom does not affect the interactions in the XB dimers. As expected, the interaction energy increases and the intermolecular distance decreases with increasing halogen atom size (Table 6).

Table 5. CP-Corrected MP2/Def2-TZVP Interaction Energies ΔE (in kcal/mol), RI-MP2/Def2-TZVP Intermolecular Distances R (in Å), and Angles θ of Activated Chalcogen-Bonded (ChB) and Halogen-Bonded (XB) Dimers Se5–Se8

ChB dimer				XB dimer			
Target	ΔE	R^a	θ^b	ΔE	R^c	$ heta^d$	θ^e
Se5	-10.79	2.85	166.48	-1.32	3.19	164.91	179.91
Se6	-12.56	2.87	165.52	-5.56	3.09	166.21	177.10
Se7	-13.20	2.86	165.44	-7.39	3.06	166.17	174.65
Se8	-13.84	2.86	165.45	-9.78	3.05	166.22	170.62

 $[^]a$ Se---N distance. b N---SeN angle. c X---N distance. d C−X---N XB angle. e C≡C−X bend angle.

Table 6. CP-Corrected MP2/Def2-TZVP Interaction Energies ΔE (in kcal/mol), RI-MP2/Def2-TZVP Intermolecular Distances R (in Å) and Angles θ (in deg) of Activated Chalcogen-Bonded (ChB) and Halogen-Bonded (XB) Dimers Te5—Te8

	ChB dimer			XB dimer			
Target	ΔE	R^a	θ^b	ΔE	R^c	$ heta^d$	θ^e
Te5	-20.52	2.70	158.07	-1.28	3.20	165.09	180.00
Te6	-22.64	2.71	157.70	-5.69	3.07	166.59	176.50
Te7	-23.34	2.71	157.68	-7.68	3.03	166.72	173.66
Te8	-24.15	2.70	157.65	-10.43	3.00	167.20	169.05

^aTe---N distance. ^bN---TeN angle. ^cX---N distance. ^dC-X---N XB angle. ^eC \equiv C-X bend angle.

DISCUSSION

Chalcogen-Bonded Dimers. On the basis of the systematic examination of experimental and computed geometric parameters and a detailed energy decomposition analysis, we can now propose an explanation for the observed energy trends. First, the identity of the chalcogen atom strongly affects the strength of the Ch---N interaction in the chalcogen-bonded dimers. The increasingly positive σ -hole in the order S < Se < Te enhances electrostatic forces. In fact, when the chalcogen atom is changed from S to Te, the electrostatic/polarization contribution to the total interaction energy increases by about 50 kcal/mol for the nonactivated and activated systems (Figures 3 and 8). This increase in electrostatic/polarization forces is partially compensated for by an increase in the exchange-repulsion energy of ~45 kcal/mol, most likely due to increasing steric hindrance between larger chalcogen atoms. While not as significant as the electrostatic/polarization contributions, an increase in the attractive dispersion energy of about 10 kcal/mol (due to the increasing polarizability of the chalcogen atom) further stabilizes the chalcogen bond. The increasingly positive σ -hole potential with increasing chalcogen size therefore induces a reduction of the Ch---N distance and of the N---Ch-N angle.

While the nature of the chalcogen atom has a large effect on the interactions that occur in the ChB dimer, changing the halogen atom has a more subtle influence. For the activated systems, increasing the size of the halogen atom increases the interaction energy by 2–4 kcal/mol, mostly driven by dispersion (due to the higher polarizability of the larger halogen atoms) (Figure 8 and Tables 4–6). However, the structural features of the dimers mostly remain constant. For the nonactivated systems, changing the identity of the halogen atom leads to some unexpected structural and energetic changes. The attractive Ch---N σ -hole interactions that tend to bring the molecules closer also brings the Ch---X atom pair and the Ch---Ch atom pair closer together (Figure 11).

In the ChB nonactivated systems, the exchange repulsion between atoms becomes larger with increasing halogen/chalcogen size as the molecules get closer (Tables S1 and S2), except within the tellurium series, where the exchange repulsion decreases with increasing halogen size from F to I in Te1 to Te4 (Table S3). Interestingly, it is also only within this same tellurium series where we see an actual van der Waals overlap between the tellurium atom of one molecule and the halogen atom of the adjacent molecule in the ChB dimer (Figure 11, green line), as observed by the positive percent reduction in their combined Ch---X vdW radii (Table S13). Tellurium atoms also have the largest σ -holes, spanning almost the entire surface of the atom, as observed from their electron density maps (Figure S1). All of these facts combined can help rationalize the unusual reduction in exchange repulsion with

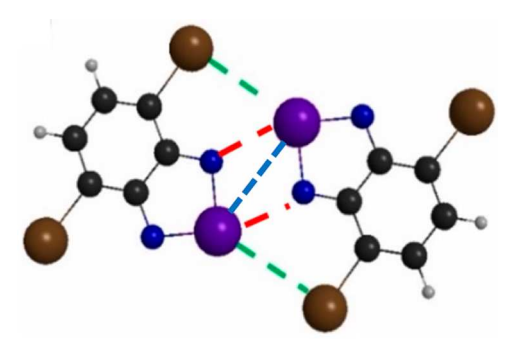


Figure 11. Attractive Ch---N (red dashed line) interactions also bring the Ch---X (green dashed line) and Ch---Ch (blue dashed line) atom pairs closer together in the optimized nonactivated ChB dimer. Color code: black, carbon; blue, nitrogen; white, hydrogen; purple, chalcogen atom Ch (S, Se, or Te); brown, halogen atom X (F, Cl, Br, or I).

increasing atomic overlap and halogen atom size in the tellurium series. We hypothesize that the large circumference of the σ -hole on the tellurium atom allows the larger chalcogen to rearrange its orientation and hence promote an attractive stabilizing interaction between the electron-deficient regions around the σ -hole and the electron-rich region around the overlapping halogen atom, resulting in an overall decreasing repulsion between the two molecules with increasing halogen atom size

While the Ch---Ch steric interaction (Figure 11, blue line) becomes more repulsive as the chalcogen atom becomes larger (Table S13), it is unlikely to be the driving force behind the observed energy trends in comparison to the Ch---X steric interactions (Figure 11, green line). First, the Ch---X atomic overlap increases to become almost similar to the Ch---Ch atomic overlap for the larger chalcogen atoms, as observed from the percent reduction in the vdW radii (Table S13). Second, for the activated systems, a smooth increase in interaction energy and exchange repulsion is observed for all three chalcogen atoms as the halogen atoms change from X = F to X = I (Tables 4–6 and Tables S4–S6). For these systems, the same Ch---Ch interaction is present but there are no Ch----X steric effects. This suggests that the Ch----X interaction becomes more prominent as the chalcogen atoms become larger.

Halogen-Bonded Dimers. Interaction energies of halogen-bonded dimers are generally weaker than those obtained for chalcogen-bonded dimers. As shown in Figure 12, the energy difference between the two conformers (circles and triangles) rapidly increases with increasing chalcogen atom size (red to green to blue, up to \sim 20 kcal/mol difference for Ch = Te). However, the activation of the halogen atoms strengthens the halogen bond by \sim 3–7 kcal/mol. For the sulfur series, the

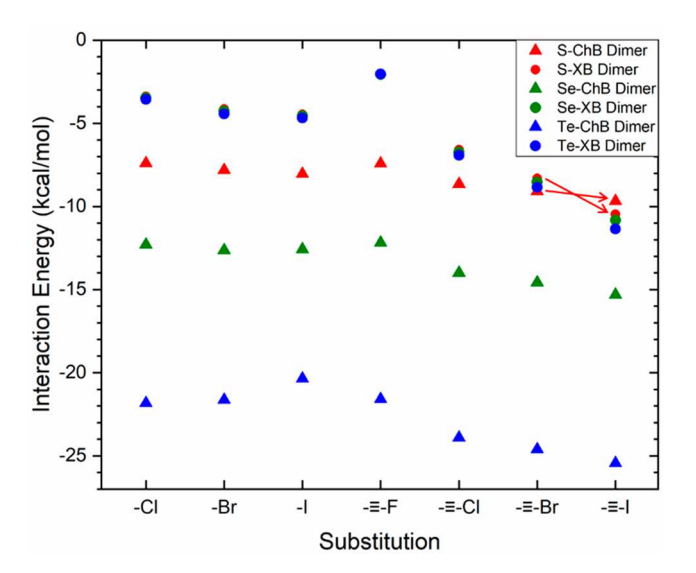


Figure 12. Interaction energies calculated for ChB dimers and XB dimers of variously substituted S, Se, and Te targets. Color and symbol code: red, sulfur targets; green, selenium targets; blue, tellurium targets; triangles, ChB dimers; circles, XB dimers. Red arrows point to the calculations predicting the switch of the most stable dimer from the ChB dimer to the XB dimer in **S8**, as confirmed by its crystal structure (Figure 7d).

XB interaction then becomes competitive and similar in magnitude to the ChB interaction (Table 4). Furthermore, for S8 with Ch = S and X = I, the halogen-bonded dimer even becomes slightly lower in energy than the chalcogen-bonded dimer, an accurate prediction in comparison to the experimental crystal structure of S8 (Figures 7d and 12). This reversal in trend is made possible because of the bending of the C≡C-X bond in the activated systems predicted in calculations and observed in the experimental crystal structure (Figure 7d, Table 4 and Table S14), which facilitates the σ hole interaction to take place. The intermolecular interaction energy of the XB dimer becomes larger in the order Cl < Br < I, due to the increasing electrostatic/polarization σ -hole and dispersion forces. These trends are amplified in the activated series of molecules (Figures 4 and 9). The nature of the chalcogen atom has no significant effect on the strength of the X---N interaction in the XB dimers, as expected.

CONCLUSIONS

In summary, we have demonstrated that organic crystalline solids with specific structural features can be constructed by exploiting and fine-tuning the competition between different σ hole interactions such as halogen and chalcogen bonds. The starting point for this systematic synthetic and computational effort was a benzochalcogenadiazole core which typically selfassembles into dimers in the solid state via two S---N chalcogen bonds. However, by introducing competing halogen-bond donors of increasing polarizability, Cl < Br < I, and by activating these donors through adjacent sp-hybridized carbon atoms, we were able to push the system beyond a tipping point whereby the latter σ -hole interactions took on a more dominant role. As a result, the structural outcome completely changed leading to the presence of halogen-bonded dimers with very different structural metrics. We subsequently increased the strength of the chalcogen bonds, via a selenium for sulfur substitution in the benzochalcogenadiazole backbone, which turned the supramolecular balance back in favor of the ChB-driven dimers. The experimental work was successfully reflected by the results obtained from state of the art ab initio calculations. Not only were structural trends accurately mapped out but also a number of detailed geometric features in the experimentally observed crystal structures could be predicted and rationalized by the computational work. The multidisciplinary approach presented herein provides an effective blueprint for how we can deliberately manipulate the delicate balance between two closely related σ -hole interactions in order to program and direct different selfassembly paths through subtle covalent modifications. From a practical point of view, this may facilitate more effective and robust bottom-up approaches to materials design, where specific architectural features are required in order to deliver function and performance in the resulting bulk material.

ASSOCIATED CONTENT

Supporting Information

The Supporting Information is available free of charge at https://pubs.acs.org/doi/10.1021/acs.cgd.1c01023.

Synthesis schemes, monomer electron density maps, Mulliken charges, electrostatic potentials, Ch−Ch and Ch−X distances in nonactivated ChB dimers, an analysis of steric effects in nonactivated dimers, effect of C≡C−X bending on the stabilization of the halogen bond, CP corrected and noncorrected MP2 energy decomposition analysis of all dimers, and the atomic coordinates of all RI-MP2/Def2-TZVP optimized monomers and dimers (PDF)

Accession Codes

CCDC 2089916, 2089920–2089922, 2089924, 2089930, 2089933, and 2089936 contain the supplementary crystallographic data for this paper. These data can be obtained free of charge via www.ccdc.cam.ac.uk/data_request/cif, or by emailing data_request@ccdc.cam.ac.uk, or by contacting The Cambridge Crystallographic Data Centre, 12 Union Road, Cambridge CB2 1EZ, UK; fax: +44 1223 336033.

AUTHOR INFORMATION

Corresponding Authors

Emilie B. Guidez – Department of Chemistry, University of Colorado, Denver, Colorado 80217, United States;

orcid.org/0000-0003-1961-0469; Email: emilie.guidez@ucdenver.edu

Christer B. Aakeröy — Department of Chemistry, Kansas State University, Manhattan, Kansas 66506, United States; orcid.org/0000-0002-8947-2068; Email: aakeroy@ksu.edu

Authors

Vinu V. Panikkattu — Department of Chemistry, Kansas State University, Manhattan, Kansas 66506, United States; orcid.org/0000-0001-7498-3722

Anh Tran — Department of Chemistry, University of Colorado, Denver, Colorado 80217, United States; ocid.org/0000-0001-5367-1682

Abhijeet S. Sinha — Department of Chemistry, Kansas State University, Manhattan, Kansas 66506, United States;
Occid.org/0000-0001-5610-2848

Eric W. Reinheimer – Rigaku Americas Corporation, The Woodlands, Texas 77381, United States

Complete contact information is available at: https://pubs.acs.org/10.1021/acs.cgd.1c01023

Author Contributions

The manuscript was written through contributions of all authors. All authors have given approval to the final version of the manuscript.

Notes

The authors declare no competing financial interest.

■ ACKNOWLEDGMENTS

This research was funded by the CU Denver Eureka and UROP programs. We acknowledge the NSF-MRI grant CHE-2018414, which was used to purchase the single-crystal X-ray diffractometer and associated software employed in this study.

REFERENCES

- (1) Wang, Y.; Sun, L.; Wang, C.; Yang, F.; Ren, X.; Zhang, X.; Dong, H.; Hu, W. Organic crystalline materials in flexible electronics. *Chem. Soc. Rev.* **2019**, 48 (6), 1492–1530.
- (2) Maharramov, A. M.; Mahmudov, K. T.; Kopylovich, M. N.; Pombeiro, A. J. Non-covalent interactions in the synthesis and design of new compounds; Wiley Online Library: 2016.
- (3) Corpinot, M. K.; Bučar, D.-K. A Practical Guide to the Design of Molecular Crystals. Cryst. Growth Des. 2019, 19 (2), 1426–1453.
- (4) Cherukuvada, S.; Kaur, R.; Guru Row, T. N. Co-crystallization and small molecule crystal form diversity: from pharmaceutical to materials applications. *CrystEngComm* **2016**, *18* (44), 8528–8555.
- (5) Aakeröy, C. B.; Sinha, A. S. Co-crystals: preparation, characterization and applications; Royal Society of Chemistry: 2018; Vol. 24.
- (6) Gunawardana, C. A.; Desper, J.; Sinha, A. S.; Đaković, M.; Aakeröy, C. B. Competition and selectivity in supramolecular synthesis: structural landscape around 1-(pyridylmethyl)-2,2'-biimidazoles. *Faraday Discuss.* **2017**, 203 (0), 371–388.
- (7) Ariga, K. Nanoarchitectonics: a navigator from materials to life. *Materials Chemistry Frontiers* **2017**, 1 (2), 208–211.
- (8) Ariga, K.; Ji, Q.; Nakanishi, W.; Hill, J. P.; Aono, M. Nanoarchitectonics: a new materials horizon for nanotechnology. *Mater. Horiz.* **2015**, 2 (4), 406–413.
- (9) Ariga, K.; Jia, X.; Song, J.; Hill, J. P.; Leong, D. T.; Jia, Y.; Li, J. Nanoarchitectonics beyond Self-Assembly: Challenges to Create Bio-Like Hierarchic Organization. *Angew. Chem., Int. Ed.* **2020**, *59* (36), 15424–15446.
- (10) Armstrong, G.; Buggy, M. Hydrogen-bonded supramolecular polymers: A literature review. J. Mater. Sci. 2005, 40 (3), 547–559.
- (11) Prins, L. J.; Reinhoudt, D. N.; Timmerman, P. Noncovalent Synthesis Using Hydrogen Bonding. *Angew. Chem., Int. Ed.* **2001**, 40 (13), 2382–2426.
- (12) Wang, H.; Wang, W.; Jin, W. J. σ -Hole Bond vs π -Hole Bond: A Comparison Based on Halogen Bond. *Chem. Rev.* **2016**, *116* (9), 5072–5104.
- (13) Eraković, M.; Cinčić, D.; Molčanov, K.; Stilinović, V. A Crystallographic Charge Density Study of the Partial Covalent Nature of Strong N.-Br Halogen Bonds. *Angew. Chem., Int. Ed.* **2019**, 58 (44), 15702–15706.
- (14) Kumar, V.; Leroy, C.; Bryce, D. L. Halide ion recognition via chalcogen bonding in the solid state and in solution. Directionality and linearity. *CrystEngComm* **2018**, *20* (41), 6406–6411.
- (15) Scilabra, P.; Terraneo, G.; Resnati, G. The Chalcogen Bond in Crystalline Solids: A World Parallel to Halogen Bond. *Acc. Chem. Res.* **2019**, 52 (5), 1313–1324.
- (16) Benz, S.; Poblador-Bahamonde, A. I.; Low-Ders, N.; Matile, S. Catalysis with Pnictogen, Chalcogen, and Halogen Bonds. *Angew. Chem., Int. Ed.* **2018**, *57* (19), 5408–5412.
- (17) Lim, J. Y. C.; Beer, P. D. Sigma-Hole Interactions in Anion Recognition. *Chem.* **2018**, *4* (4), 731–783.

- (18) Lee, J.; Lee, L. M.; Arnott, Z.; Jenkins, H.; Britten, J. F.; Vargas-Baca, I. Sigma-hole interactions in the molecular and crystal structures of N-boryl benzo-2,1,3-selenadiazoles. *New J. Chem.* **2018**, 42 (13), 10555–10562.
- (19) Dong, W.; Li, Q.; Scheiner, S. Comparative Strengths of Tetrel, Pnicogen, Chalcogen, and Halogen Bonds and Contributing Factors. *Molecules* **2018**, 23 (7), 1681.
- (20) Scheiner, S.; Lu, J. Halogen, Chalcogen, and Pnicogen Bonding Involving Hypervalent Atoms. *Chem. Eur. J.* **2018**, 24 (32), 8167–8177.
- (21) Kolář, M. H.; Hobza, P. Computer Modeling of Halogen Bonds and Other σ -Hole Interactions. *Chem. Rev.* **2016**, *116* (9), 5155–5187.
- (22) Bialas, D.; Kirchner, E.; Röhr, M. I. S.; Würthner, F. Perspectives in Dye Chemistry: A Rational Approach toward Functional Materials by Understanding the Aggregate State. *J. Am. Chem. Soc.* **2021**, *143* (12), 4500–4518.
- (23) Otte, F.; Kleinheider, J.; Hiller, W.; Wang, R.; Englert, U.; Strohmann, C. Weak yet Decisive: Molecular Halogen Bond and Competing Weak Interactions of Iodobenzene and Quinuclidine. *J. Am. Chem. Soc.* **2021**, *143* (11), 4133–4137.
- (24) Xia, D.; Wang, P.; Ji, X.; Khashab, N. M.; Sessler, J. L.; Huang, F. Functional Supramolecular Polymeric Networks: The Marriage of Covalent Polymers and Macrocycle-Based Host—Guest Interactions. *Chem. Rev.* **2020**, *120* (13), 6070—6123.
- (25) Wang, W.; Ji, B.; Zhang, Y. Chalcogen Bond: A Sister Noncovalent Bond to Halogen Bond. J. Phys. Chem. A 2009, 113 (28), 8132–8135.
- (26) Adhikari, U.; Scheiner, S. Effects of Charge and Substituent on the S···N Chalcogen Bond. *J. Phys. Chem. A* **2014**, *118* (17), 3183–3192.
- (27) Luzzati, V. Structure cristalline de piasélénol, piazthiol et benzofurazane. *Acta Crystallogr.* **1951**, *4* (3), 193–200.
- (28) Brinck, T.; Murray, J. S.; Politzer, P. Surface electrostatic potentials of halogenated methanes as indicators of directional intermolecular interactions. *Int. J. Quantum Chem.* **1992**, 44 (S19), 57–64.
- (29) Politzer, P.; Murray, J. S.; Clark, T. Halogen bonding: an electrostatically-driven highly directional noncovalent interaction. *Phys. Chem. Chem. Phys.* **2010**, *12* (28), 7748–7757.
- (30) Clark, T.; Hennemann, M.; Murray, J. S.; Politzer, P. Halogen bonding: the *σ*-hole. *J. Mol. Model.* **2007**, *13* (2), 291–296.
- (31) Kolář, M. H.; Carloni, P.; Hobza, P. Statistical analysis of σ -holes: a novel complementary view on halogen bonding. *Phys. Chem. Chem. Phys.* **2014**, *16* (36), 19111–19114.
- (32) Cavallo, G.; Metrangolo, P.; Milani, R.; Pilati, T.; Priimagi, A.; Resnati, G.; Terraneo, G. The Halogen Bond. *Chem. Rev.* **2016**, *116* (4), 2478–2601.
- (33) Aakeröy, C. B.; Wijethunga, T. K.; Desper, J.; Đaković, M. Electrostatic Potential Differences and Halogen-Bond Selectivity. *Cryst. Growth Des.* **2016**, *16* (5), 2662–2670.
- (34) Wang, C.; Danovich, D.; Mo, Y.; Shaik, S. On The Nature of the Halogen Bond. *J. Chem. Theory Comput.* **2014**, *10* (9), 3726–3737.
- (35) Tomura, M.; Akhtaruzzaman, M.; Suzuki, K.; Yamashita, Y. 4, 7-Diiodo-2, 1, 3-benzothiadiazole and 7, 7'-diiodo-4, 4'-bi (2, 1, 3-benzothiadiazole). *Acta Crystallogr., Sect. C: Cryst. Struct. Commun.* **2002**, 58 (7), o373-o375.
- (36) Tomura, M.; Yamashita, Y. Crystal structure of 4,7-dibromo-2,1,3-benzothiadiazole, C6H2Br2N2S. Z. Kristallogr. New Cryst. Struct. 2003, 218 (4), 555–556.
- (37) Cozzolino, A. F.; Britten, J. F.; Vargas-Baca, I. The Effect of Steric Hindrance on the Association of Telluradiazoles through Te-N Secondary Bonding Interactions. *Cryst. Growth Des.* **2006**, *6* (1), 181–186.
- (38) Schmidt, M. W.; Baldridge, K. K.; Boatz, J. A.; Elbert, S. T.; Gordon, M. S.; Jensen, J. H.; Koseki, S.; Matsunaga, N.; Nguyen, K. A.; Su, S.; Windus, T. L.; Dupuis, M.; Montgomery, J. A. General

- atomic and molecular electronic structure system. J. Comput. Chem. 1993, 14 (11), 1347–1363.
- (39) Gordon, M. S.; Schmidt, M. W. Advances in electronic structure theory: GAMESS a decade later. In *Theory and applications of computational chemistry*; Elsevier: 2005; pp 1167–1189.
- (40) Barca, G. M. J.; Bertoni, C.; Carrington, L.; Datta, D.; Silva, N. D.; Deustua, J. E.; Fedorov, D. G.; Gour, J. R.; Gunina, A. O.; Guidez, E.; Harville, T.; Irle, S.; Ivanic, J.; Kowalski, K.; Leang, S. S.; Li, H.; Li, W.; Lutz, J. J.; Magoulas, I.; Mato, J.; Mironov, V.; Nakata, H.; Pham, B. Q.; Piecuch, P.; Poole, D.; Pruitt, S. R.; Rendell, A. P.; Roskop, L. B.; Ruedenberg, K.; Sattasathuchana, T.; Schmidt, M. W.; Shen, J.; Slipchenko, L.; Sosonkina, M.; Sundriyal, V.; Tiwari, A.; Vallejo, J. L. G.; Westheimer, B.; Włoch, M.; Xu, P.; Zahariev, F.; Gordon, M. S. Recent developments in the general atomic and molecular electronic structure system. *J. Chem. Phys.* **2020**, *152* (15), 154102.
- (41) Whitten, J. L. Coulombic potential energy integrals and approximations. J. Chem. Phys. 1973, 58 (10), 4496–4501.
- (42) Pham, B. Q.; Gordon, M. S. Hybrid Distributed/Shared Memory Model for the RI-MP2Method in the Fragment Molecular Orbital Framework. *J. Chem. Theory Comput.* **2019**, *15* (10), 5252–5258.
- (43) Weigend, F.; Häser, M. RI-MP2: first derivatives and global consistency. *Theor. Chem. Acc.* **1997**, 97 (1), 331–340.
- (44) Weigend, F.; Ahlrichs, R. Balanced basis sets of split valence, triple zeta valence and quadruple zeta valence quality for H to Rn: Design and assessment of accuracy. *Phys. Chem. Chem. Phys.* **2005**, 7 (18), 3297–3305.
- (45) Pritchard, B. P.; Altarawy, D.; Didier, B.; Gibson, T. D.; Windus, T. L. New Basis Set Exchange: An Open, Up-to-Date Resource for the Molecular Sciences Community. *J. Chem. Inf. Model.* **2019**, *59* (11), 4814–4820.
- (46) Peterson, K. A. Systematically convergent basis sets with relativistic pseudopotentials. I. Correlation consistent basis sets for the post-d group 13–15 elements. *J. Chem. Phys.* **2003**, *119* (21), 11099–11112
- (47) Su, P.; Li, H. Energy decomposition analysis of covalent bonds and intermolecular interactions. *J. Chem. Phys.* **2009**, *131* (1), 014102.
- (48) Boys, S. F.; Bernardi, F. The calculation of small molecular interactions by the differences of separate total energies. Some procedures with reduced errors. *Mol. Phys.* **1970**, *19* (4), 553–566.
- (49) Piña, M. d. l. N.; Frontera, A.; Bauza, A. Charge Assisted S/Se Chalcogen Bonds in SAM Riboswitches: A Combined PDB and ab Initio Study. ACS Chem. Biol. 2021, 16 (9), 1701–1708.
- (50) Bauzá, A.; Frontera, A. Halogen and Chalcogen Bond Energies Evaluated Using Electron Density Properties. *ChemPhysChem* **2020**, 21 (1), 26–31.
- (51) Franconetti, A.; Quiñonero, D.; Frontera, A.; Resnati, G. Unexpected chalcogen bonds in tetravalent sulfur compounds. *Phys. Chem. Chem. Phys.* **2019**, *21* (21), 11313–11319.
- (52) Bauzá, A.; Alkorta, I.; Frontera, A.; Elguero, J. On the Reliability of Pure and Hybrid DFT Methods for the Evaluation of Halogen, Chalcogen, and Pnicogen Bonds Involving Anionic and Neutral Electron Donors. *J. Chem. Theory Comput.* **2013**, 9 (11), 5201–5210.
- (53) Bondi, A. van der Waals Volumes and Radii. J. Phys. Chem. 1964, 68 (3), 441-451.
- (54) Mukherjee, A.; Tothadi, S.; Desiraju, G. R. Halogen Bonds in Crystal Engineering: Like Hydrogen Bonds yet Different. *Acc. Chem. Res.* **2014**, *47* (8), 2514–2524.
- (55) Murray, J. S.; Lane, P.; Clark, T.; Politzer, P. σ-hole bonding: molecules containing group VI atoms. *J. Mol. Model.* **2007**, *13* (10), 1033–1038.
- (56) Mulliken, R. S. Electronic Population Analysis on LCAO-MO Molecular Wave Functions. I. *J. Chem. Phys.* **1955**, 23 (10), 1833–1840.
- (57) Risto, M.; Assoud, A.; Winter, S. M.; Oilunkaniemi, R.; Laitinen, R. S.; Oakley, R. T. Heavy Atom Analogues of 1,2,3-Dithiazolylium Salts: Preparation, Structures and Redox Chemistry. *Inorg. Chem.* **2008**, 47 (21), 10100–10109.